High-performance $Li_{1.2}Mn_{0.6}Ni_{0.2}O_2$ cathode materials prepared through a facile one-pot co-precipitation process for lithium ion batteries

Nomasonto Rapulenyane [a,b], Ernst Ferg [b], Bonani Seteni [a], Hongze Luo [a]*

[a] *Council for Scientific and Industrial Research, Pretoria 0001, South Africa*

[b] *Department of Chemistry, Nelson Mandela Metropolitan University, Port Elizabeth 6031, South Africa*

** Corresponding author e-mail:hluo@csir.co.za, hongzee@gmail.com*

Tel: +2712 841 2389; Fax: +2712 841 2135.

Abstract

In a quest to produce cathode materials for lithium ion batteries that yield high capacities, the $Li_{1.2}Mn_{0.6}Ni_{0.2}O_2$, lithium-manganese rich cathode materials were synthesized via a facile one-pot co-precipitation process with various ratios of urea at pH 9.0, 9.5, 10.0 and 10.5. The physical properties of the cathode materials were analysed by X-ray diffraction, Brunauer–Emmett–Teller surface area, scanning electron microscopy, transmission electron microscopy, inductively coupled plasma mass spectrometry and energy dispersive spectroscopy. The X-ray diffraction study showed that the prepared materials were crystalline with an ordered layered structure in the respective unit cell parameters being indexed to a monoclinic $C_{2/c}$ space group. Scanning electron microscopy showed that $Li_{1.2}Mn_{0.6}Ni_{0.2}O_2$ particles are agglomerated, however pH 10.0 particles appear less agglomerated and possess a slightly higher surface area. The cathode materials were built into coin cells and displayed exceptional electrochemical performance in delivering more than 200 mAh g^{-1} at a constant current density of 20 mA g^{-1} in the voltage range of 2.0 V-4.8 V. In particular the cathode

material made at pH 10.0 delivered an initial high discharge capacity of 266 mAh g^{-1} at 20 mA g^{-1} current density and maintained a discharge capacity of more than 220 mAh g^{-1} at 50 mA g^{-1} after 50 cycles.

Keywords: lithium ion battery, lithium-rich cathode, co-precipitation, $Li_{1.2}Mn_{0.6}Ni_{0.2}O_2$

1. Introduction

Lithium ion batteries (LIBs) have been a dominant power source for a wide range of portable electronic devices such as laptops, power tools and mobile phones. Since the inception of commercialization of rechargeable batteries by Sony in 1991, the layered $LiCoO_2$ was the most widely used cathode material for the LIBs in many portable electronics due to its excellent capacity rate capabilities, cycling performance and a material that has a high-tap density [1, 2]. However, the high cost and safety concerns of using cobalt as the cathode material has led to research of alternative cathode materials that are cheaper that also have higher specific capacities and could operate at higher potentials when compared to the cobalt based oxides [3]. Spinel $LiMn_2O_4$ was one of the first alternative cathode materials to $LiCoO_2$ because of its lower material cost with less environmental concerns [4]. However, its specific capacity of 120 mAh g^{-1} at 4.1 V vs. Li^0/Li^+ with poor cycling performance has limited its use in lithium ion batteries [5].

The search for higher density electrode material with excellent electrochemical output is becoming more crucial due to expansion of lithium ion battery applications for advanced energy storage devices such as electric vehicles (EV) and hybrid electric vehicles (HEV) [6, 7]. In order to improve the electrochemical stability of the manganese based spinel material, many elemental dopants have been considered that include amongst others Fe, Al, Na, Ni, Co and Zn [8-10]. Recently, Lithium-manganese-rich layered transition metal oxide (LMR-TM) composites have been promising candidates to achieve higher capacities (greater than 200 mAh g^{-1}) and voltage stabilities with good cycle life in order to provide the necessary power requirements for electric vehicles (EV) and hybrid electric vehicles (HEV) [6, 7]. The operating voltage window of these LMR-TM materials have shown to be within the high range of 2.0 V to 4.8 V [11], which is ideal for the higher power requirements associated with EV. The general chemical formula of LMR-TMs are written as xLi_2MnO_3 $(1-x)$ $LiMO_2$ where

M = Mn, Ni, Co and x between 0 and 1. The electrochemical properties of cathode materials such as capacity and cycling stability depends on various parameters such as the value of x, amounts of manganese, nickel and cobalt [12]. Ideally, the larger the value of x the more the capacity as this means the more Li_2MnO_3 component in the composite [13]. The LMR-TMs are relatively environmental benign and cost effective due to limited quantities of the cobalt used in their molecular structures and their high thermal stability on recharging [14, 15]. The LMR-TM materials offer a synergistic effect, where more Li^+ ions are able to be extracted and inserted during the charge and discharge cycling. The capacity that is produced at potentials below 4.5 V (vs Li/Li^+) can be attributed to the $LiMO_2$ component, whereas Li_2MnO_3 composite serves as a capacity reservoir when charged above 4.5 V (Li/Li^+).

Nonetheless, the LMR-TM structure is a complex structure with inherent shortcomings which include; large initial irreversible charge capacity, capacity fade upon prolonged cycling, poor continuous charge and discharge rate capability, high reactivity with the electrolyte at high voltages [16]. Synthesis methods affect the crystal formation, morphology and particle sizes of the cathode materials and subsequently the electrochemical performance of the materials [17]. Various methods such as hydrothermal [18], solid-state[19], combustion [20], co-precipitation [13] and sol-gel method [21] have been employed to produce LMR-TM materials. Co-precipitation and sol-gel synthesis methods are preferred for the preparation of these materials because they produce homogeneous and pure phase materials [22]. Co-precipitation method is already in the industry and is being used to produce precursors for commercial production of ($Li[Ni_{1/3}Co_{1/3}Mn_{1/3}]O_2$, $LiNi_{0.64}Co_{0.18}Mn_{0.18}O_2$, $LiNi_{0.83}Co_{0.07}Mn_{0.10}O_2$ and $LiNi_{0.5}Mn_{1.5}O_4$, etc) [23, 24]. Although it is also viable for large scale production of LMR-TM, the process can be improved by exploring other synthesis methods to overcome the drawbacks, such as time consumption due to the involment of multiple steps towards LMR-TM synthesis (precursor characterization before lithiation step).

A number of cathode materials with different x values have been extensively studied and x= 0.5, $0.5Li_2MnO_3.0.5LiMn_{0.5}Ni_{0.5}O_2$ which can also be written as $Li_{1.2}Mn_{0.6}Ni_{0.2}O_2$ is by far the most promising material [25-27].This article will report on the advantages of employing a one-pot co-precipitation synthesis method to make $Li_{1.2}Mn_{0.6}Ni_{0.2}O_2$ using shorter preparation times and yet delivering the good promising battery performance.

2. Experimental

2.1. Materials and Methods

$Li_{1.2}Mn_{0.6}Ni_{0.2}O_2$ cathode materials were synthesized via a facile one-pot co-precipitation method using a mixture base solution of LiOH and urea with various ratios of urea: from 1.0 to 1.8. The stoichiometric ratios of Li:Mn:Ni were kept fixed for the desired $Li_{1.2}Mn_{0.6}Ni_{0.2}O_2$, while urea was varied from 1.0 to 1.8, resulting in four batches of $Li_{1.2}Mn_{0.6}Ni_{0.2}O_2$ that changed in the respective pH namely pH 9.0 (1.0), pH 9.5 (1.2), pH 10.0 (1.6) and pH 10.5 (1.8) . A typical synthesis procedure involved dissolving appropriate stoichiometric amounts of manganese acetate tetrahydrate $Mn(CH_3COO)_2.4H_2O$ (Sigma-Aldrich) and Nickel acetate tetrahydrate $Ni(CH_3COO)_2.4H_2O$ (Sigma-Aldrich) in distilled water to make up a 0.33 molar solution. Lithium hydroxide $LiOH.H_2O$ (Sigma-Aldrich) and urea $CO(NH_2)_2$ (Merck) were dissolved separately in deionized water making 0.33 molar solution. The solutions in both beakers were stirred at 1000 rpm at 70 ˚C until completely dissolved. The metal ions acetate solution was then introduced dropwise to the base solution while stirring at 1000 rpm at 70 ˚C and the solution colour changed gradually to dark brown colour as the precipitate formed. The formed precipitate was then left stirring at 70 ˚C and then for another 10 hours to evaporate the distilled water at 100 ˚C. A fine brown powder was obtained and was subjected to 600 ℃ for 2 hours (5 ℃ min^{-1}) in an air flowing furnace to

burn off all the acetates/organics. The 2nd heating was done at higher temperatures 900 ˚C for 12 hours to promote the formation of the final proper crystalline phase.

2.2. Characterization Techniques

A ZEISS ULTRA SS (Germany) field emission scanning electron microscope (FESEM) was used for the morphological analysis of the cathode powders before cycling. The X-Max50mm^2 energy dispersive spectrometer (EDS) from the FESEM was also used to obtain a semi-qualitative elemental composition of the samples. The bright field transmission electron microscopy (TEM) (JEOL JEM-2010F) was employed to evaluate the cathode materials structure and composition. Thermo scientific iCAPQ inductively coupled plasma mass spectrometry (ICP-MS) was used to analyse the Mn and Ni atomic percentage. All four powders were digested in aqua-regia and diluted in distilled water and further diluted 1000X before analysis. The ICP multi element standard solution 1 (sigma Aldrich) was used for calibration purposes, the standard was prepared in 5 folds namely: 20, 40, 60, 80 and 100 part per billion (ppb) in 3% nitric acid. X-ray diffraction (XRD) patterns were recorded by a Bruker AXS D8 ADVANCE X-ray Diffractometer with Ni-filtered Cu Kα (λ = 5406Å). The X-ray tube operating parameters were 40 kV and 40 mA. The measurements were taken with 2 Theta (2θ) angle ranging from 10° to 90 °, with a 0.02 ° step. Rietveld refinement was achieved by using Topas 5 software, the atomic site occupancy, in particular the Ni and Li ion positions allowed for the refinement of the amount of the specific element to sit on the specific atomic coordinate. These were allowed to refine close to the $Li_{1.2}$ $Mn_{0.6}Ni_{0.2}O_2$ chemical formula [28]. Li_2MnO_3 [29] chemical formula was also used to refine the XRD patterns of the produced materials, because $Li_{1.2}$ $Mn_{0.6}Ni_{0.2}O_2$ materials have Li_2MnO_3 composite in their structure. The lattice parameter was allowed to be refined and

subsequently fixed for further analysis. The composition is determined by the semi quantitative Rietveld refinement based on the crystal structure. However, it must be remembered that there can be significant error due to the fact there is significant overlap in some of the peaks between the two compounds specifically at 2 theta 18.5˚, 37˚ and 44.5˚.

Surface area studies of the produced materials were determined using nitrogen physisorption incorporating the Brunauer-Emmett-Teller (BET) method. The measurements were recorded using a micrometric ASAT 2020 instrument physisorption analyser. The samples were pre-treated where 0.5 g of material was dried at 120 ˚C under vacuum for 2 hours prior to BET measurements.

2.3. Cell assembly and preparations

The cathode electrodes were prepared by mixing active material, carbon black and polyvinylidene fluoride in the mass ratio 8:1:1 respectively. The resulting slurry of N-Methylpyrrolidone was cast on aluminium foil and dried at 110 ˚C under vacuum. The cathode electrodes were cut to fit into 2032-type coin cells, the active material loading was 24 mg cm^{-2}. Coin cells were assembled in an argon filled glove box (Mbraun - Labstar). Lithium metal was used as an anode and $LiFP_6$ electrolyte (1 M LiPF6 in ethylene carbonate and dimethyl carbonate, 1:1 volume ratio) was used to prepare the coin cells. The coin cells were used to evaluate the electrochemical performance of the cathode materials, they were charged and discharged galvanostatically on Maccor battery tester (Series 4000) at 20 mA g^{-1} current density between 2.0 V - 4.8 V (vs Li/Li^+) at room temperature. Impedance analysis was achieved by using Biologic Science Instrument VMPS, coupled with the EC-Lab Express software. The measurements were taken between 10 MHz and 100 KHz with perturbation amplitude of the ac signal of 3 mV.

3. Results and discussion

3.1. Structure and morphology characterization

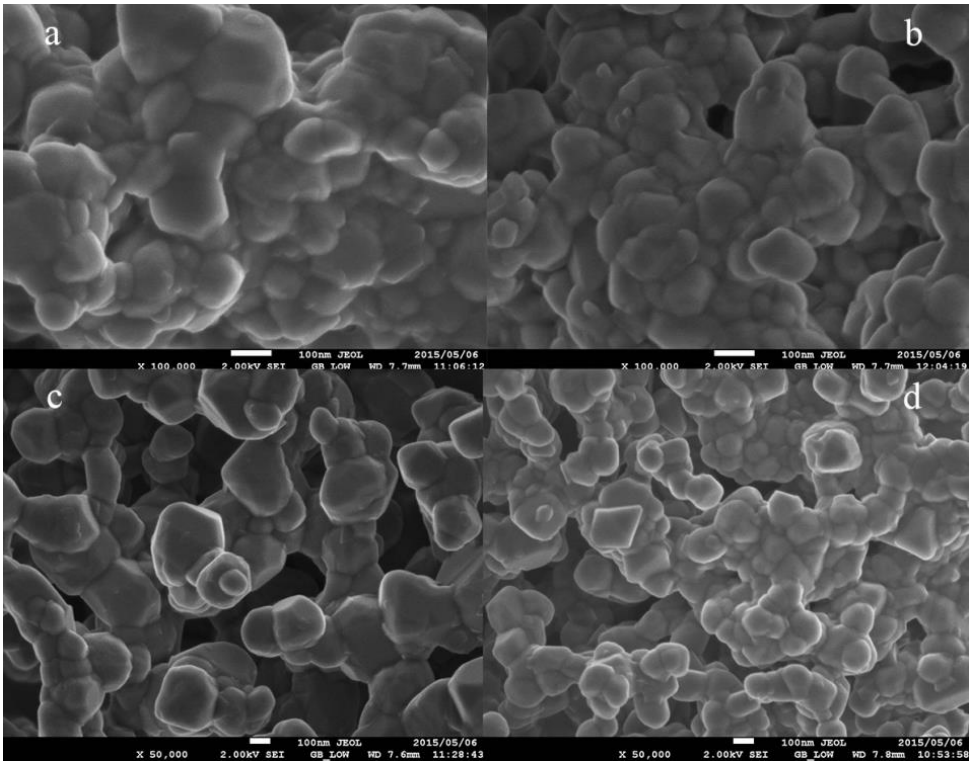

Fig. 1. SEM images of $Li_{1.2}Mn_{0.6}Ni_{0.2}O_2$, (a) pH 9.0, (b) pH 9.5, (c) pH10.0 and (d) pH 10.5 respectively.

Surface morphologies of the prepared materials characterized by FESEM, are shown in Fig. 1(a-d). Particles are highly agglomerated and assume a spherical shape. Particles pH 10.0 appears slightly less agglomerated compared to its counterparts. Three measurements were done per sample for BET, the averages and standard deviations are reported as 2.057 ± 0.3634 m^2 g^{-1}, 1.798 ± 0.262 m^2 g^{-1}, 2.120 ± 0.1955 m^2 g^{-1} and 1.7030 ± 0.264 m^2 g^{-1} for pH 9.0, 9.5, 10.0 and 10.5 respectively. As observed, BET shows that pH 10.0 sample has the largest surface area.

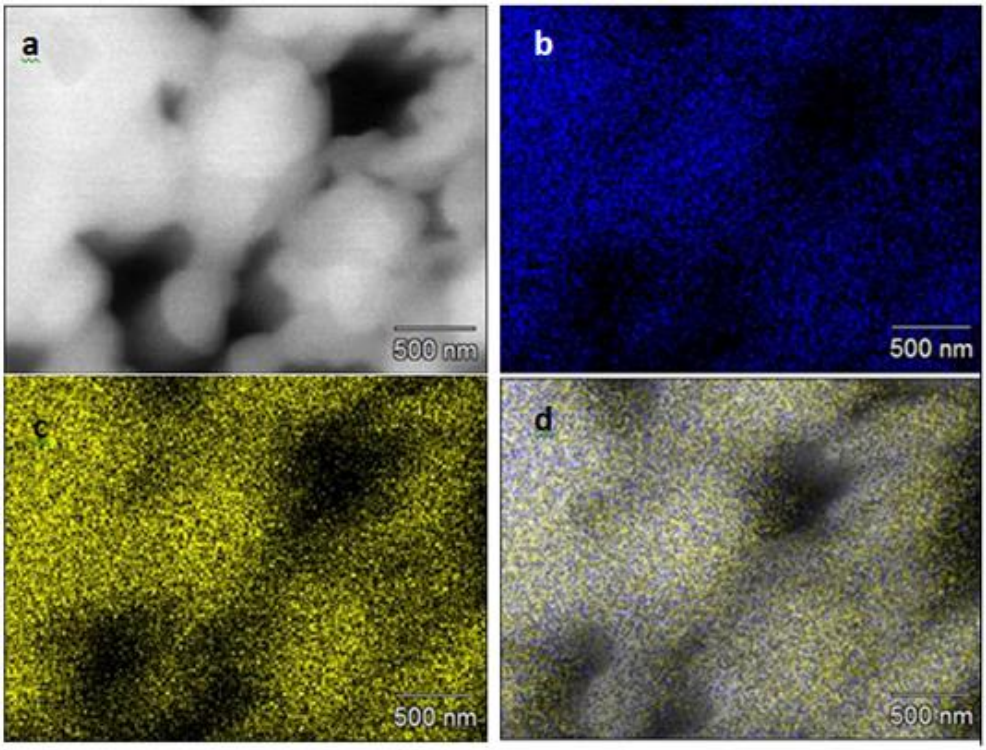

Fig. 2. EDS elemental mapping for pH 10.0 material(a) reference area of analysis, (b) Ni mapping, (c) Mn mapping and (d) Ni and Mn elemental mapping overlay.

Qualitative analysis of the transition metals composition of the prepared materials was carried out using electron diffraction spectroscopy (EDS). EDS measured the relative percentage weight of the elements present in the sample with the ability to obtain an elemental mapping (Fig. 2) that shows that the two transitional metals nickel and manganese are evenly distributed throughout the samples made at the various pHs. This therefore suggests that the synthesis method used is suitable to produce homogenous LMR-TM cathode materials.

Based on the relative energy intensities of observed elements in the EDS spectra, one can determine the Mn and Ni in the $Li_{1.2}Mn_{0.6}Ni_{0.2}O_2$ samples as expected, however due to the limitation of EDS towards low mass, lithium could not be accurately determined. The results in table 1 showed that Mn to Ni elemental ratio in the samples prepared were in reasonable agreement with the desired ratio of 3 to 1. Furthermore, the respective metal concentrations in

each sample were investigated by ICP-MS and pH 10.0 had the closest composition to the theoretical as shown in Table 2 comparing to their theoretical compositions. Three materials pH 9.0, 9.5 and 10.0 had the 3:1 elemental ratio while pH 10.5 had 2.89: 1 elemental ratio between Mn and Ni.

Table 1: showing Mn and Ni atomic percentages and the Mn:Ni ratio in each sample of $Li_{1.2}Mn_{0.6}Ni_{0.2}O_{2.}$ The desired ratio Mn:Ni = 3:1

Sample name	**Manganese (at.%)**	**Nickel (at.%)**	**Mn:Ni Ratio**
pH 9.0	26.35	8.94	2.95:1
pH 9.5	14.59	4.99	2.93:1
pH 10.0	16.83	5.55	3.03:1
pH 10.5	44.69	15.68	2.85:1

Table 2: ICP_OES results for $Li_{1.2}Mn_{0.6}Ni_{0.2}O_2$ at pH 9.0, 9.5, 10.0 and 10.5

Sample name	**Lithium**	**Manganese**	**Nickel**	**Mn:Ni Ratio**
pH 9.0	1.23	0.58	0.19	3.05:1
pH 9.5	1.24	0.57	0.19	3:1
pH 10.0	1.22	0.59	0.19	3.1:1
pH 10.5	1.26	0.55	0.19	2.89:1

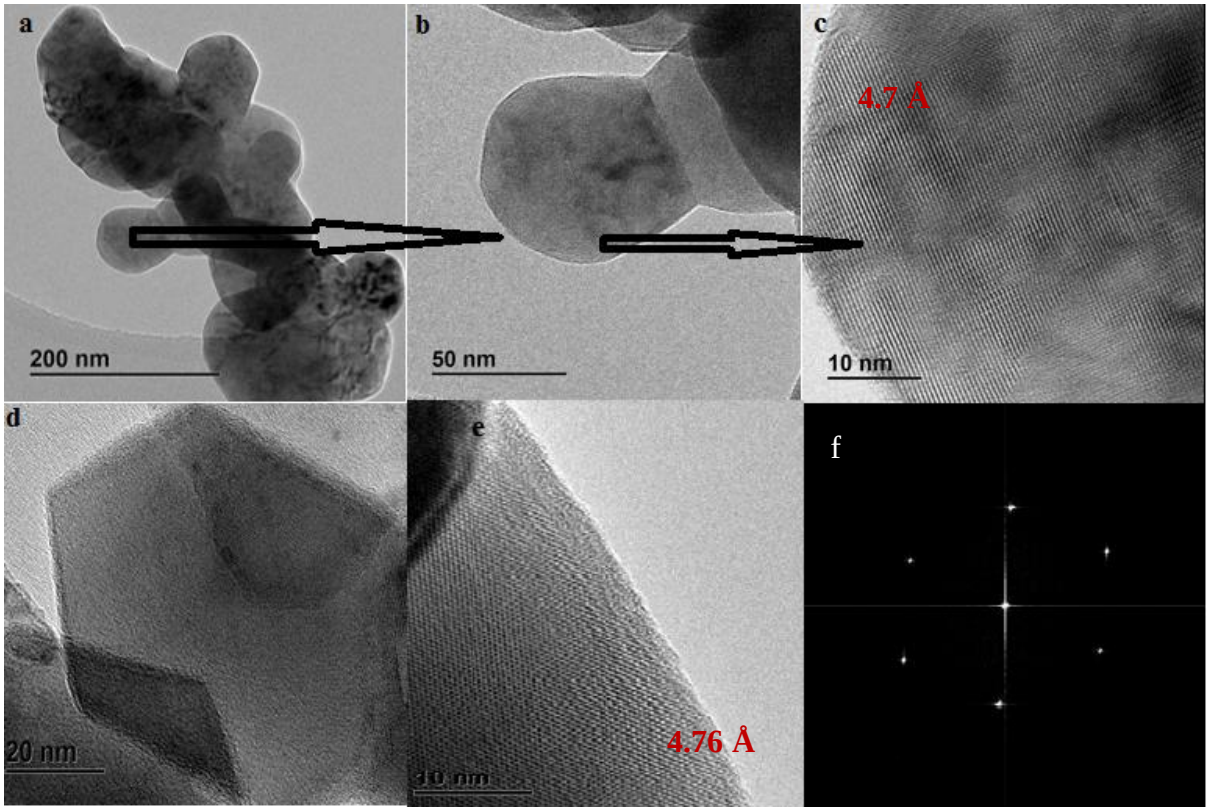

Fig.3.HRTEM morphology imaging of the as-prepared pH 10.0 (a), focus area for FFTs (b) FFTs with d-spacing from the surface of the as-prepared pH 10.0 (c), hexagonal particle image of the as-prepared pH 10.0 material, (e) FFT and the diffraction pattern (f).

TEM provided complementary results in terms of the morphology of the particles, the particles assume a spherical shape and are agglomerated (figure 3a) same as SEM results. However TEM also showed that some of the particles within the sample were hexagonal, making the materials a mixture of spherical and hexagonal particles. A selected area diffraction (SAED) pattern from the surface regions of $Li_{1.2}Mn_{0.6}Ni_{0.2}O_2$ is presented in figure 3f and show a clear hexagonal diffraction pattern. This diffraction pattern is reported in literature for both layered $Li_{1.2}Mn_{0.6}Ni_{0.2}O_2$ and $LiMn_{0.5}Ni_{0.5}O_2$ structures. This pattern observed here therefore proves the formation of the layered $Li_{1.2}Mn_{0.6}Ni_{0.2}O_2$ [30-32]. Figure 3c and eshow high-contrast lattice fringes, figure 3c show multidirectional fringes with 4.7 Å

d-spacing as measured from the lattice finges. The measured d-spacing corresponds to the close-packed planes of the composite structure, indicating good structural integration between Li_2MnO_3 and $LiMn_{0.5}Ni_{0.5}O_2$ components at atomic level as postulated by Thackeray and co-workers. The d-spacing for this composite corresponds to the reported 4.7 Å by Thackeray and co-workers [12] and also Wu and his co-workers reported the same [33-35].

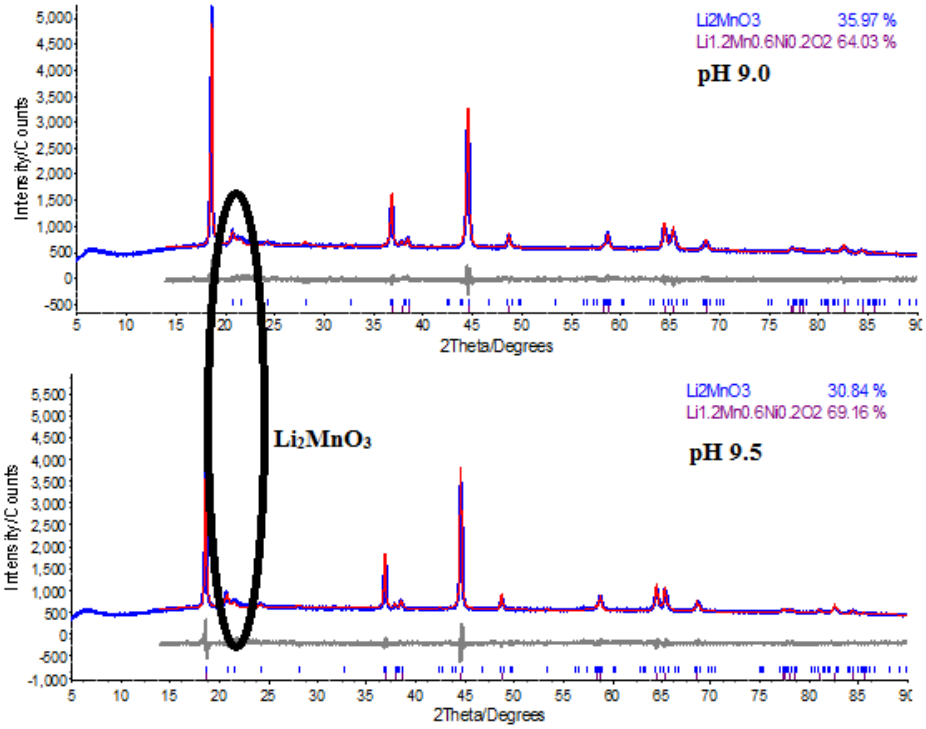

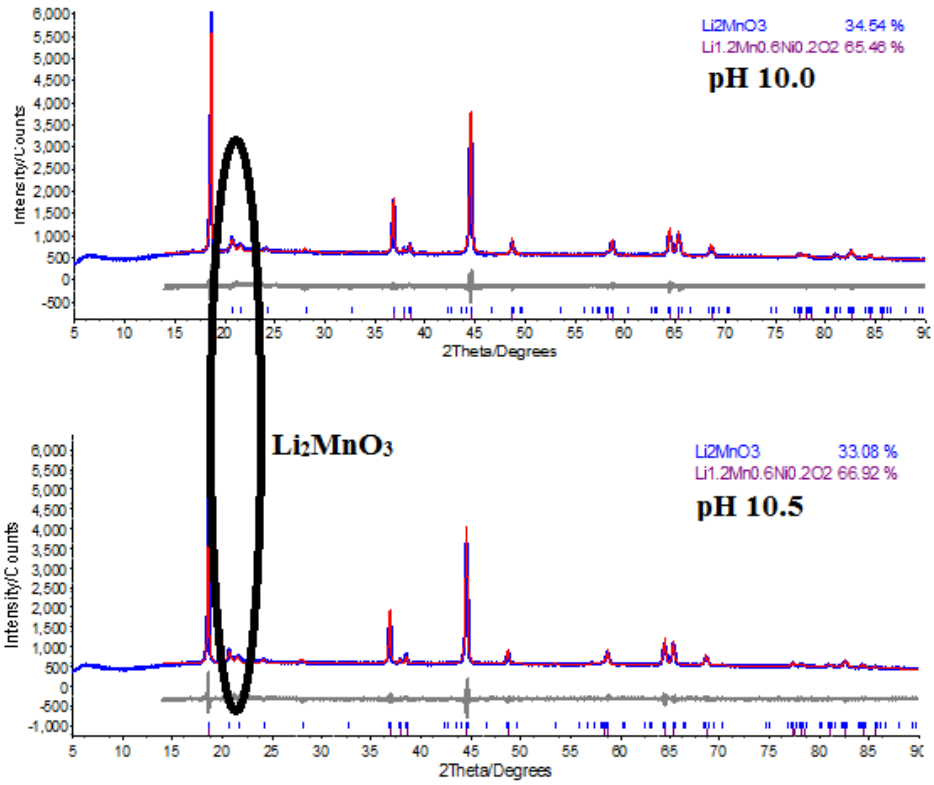

Fig. 4. XRD reflection patterns of $Li_{1.2}Mn_{0.6}Ni_{0.2}O_2$ materials and their refined results

Fig. 4 shows the various XRD patterns of the layered $Li_{1.2}Mn_{0.6}Ni_{0.2}O_2$ oxides prepared at various pH values by a facile one pot co-precipitation method and calcined at 900 ˚C. Despite the use of different ratios of urea during synthesis, the XRD patterns for $Li_{1.2}Mn_{0.6}Ni_{0.2}O_2$ oxides are all similar and corresponds to the reported patterns in literature[36-38]. The reflection patterns observed are mainly that of $Li_{1.2}Mn_{0.6}Ni_{0.2}O_2$ orthorhombic as a primary phase and monoclinic phase as a secondary phase. The reflection peaks are unique to the monoclinic Li_2MnO_3 crystalline structure are observed between 20˚ and 25˚, as highlighted by the circle in fig.4 [39, 40]. Based on these refined results the materials are therefore characterized as the combination of two phases. Table 3 below shows the phase compositions of the materials and their rietveld refined lattice parameters. The $Li_{1.2}Mn_{0.6}Ni_{0.2}O_2$ at pH 9.0, pH 9.5 and 10.0 consists of about 35% monoclinic phase as a secondary phase whereas pH 10.5 has less monoclinic phase (32.05%). Cell parameters calculated using Rietveld

refinements were found to be all the same for the monoclinic phase and slightly different for the orthorhombic phase as reported in table 3 from both crystal structures. The lattice parameters obtained for the orthorhombic phase are similar to those reported for $LiMn_{0.5}Ni_{0.5}O_2$ [41] and those for the monoclinic phase are also same to those in reported in literature[32]. The crystal sizes as determined by the XRD increases with pH for both phases, the monoclinic phase possess small crystal size compared to the orthorhombic phase.

Table 3: Rietveld refinement results

Sample	**a (Å) monoclinic**	**c (Å) monoclinic**	**a (Å) orthorhombic**	**c (Å) orthorhombic**	**Crystal size/ LVol-FWHM (nm)**	**Rwp %**	**Crystal compositio**
pH 9.0	2.85	14.23	4.97	5.00	133.88 nm (orthorhombic) 18.84 nm (monoclinic)	3.12	Orthorhombic 64.07 Monoclinic 35.93%
pH 9.5	2.85	14.23	4.94	5.02	164.82 nm (orthorhombic) 24.55 nm (monoclinic)	3.35	Orthorhombic 64.86 Monoclinic 35.14%
pH 10.0	2.85	14.23	4.95	5.03	176.8 nm (orthorhombic) 27.1 nm (monoclinic)	3.23	Orthorhombic 65.46 Monoclinic 35.54%
pH 10.5	2.85	14.23	4.94	5.03	237.3 nm (orthorhombic) 28.1 nm (monoclinic)	3.49	Orthorhombic 67.95 Monoclinic 32.05%

3.2. Electrochemical measurements

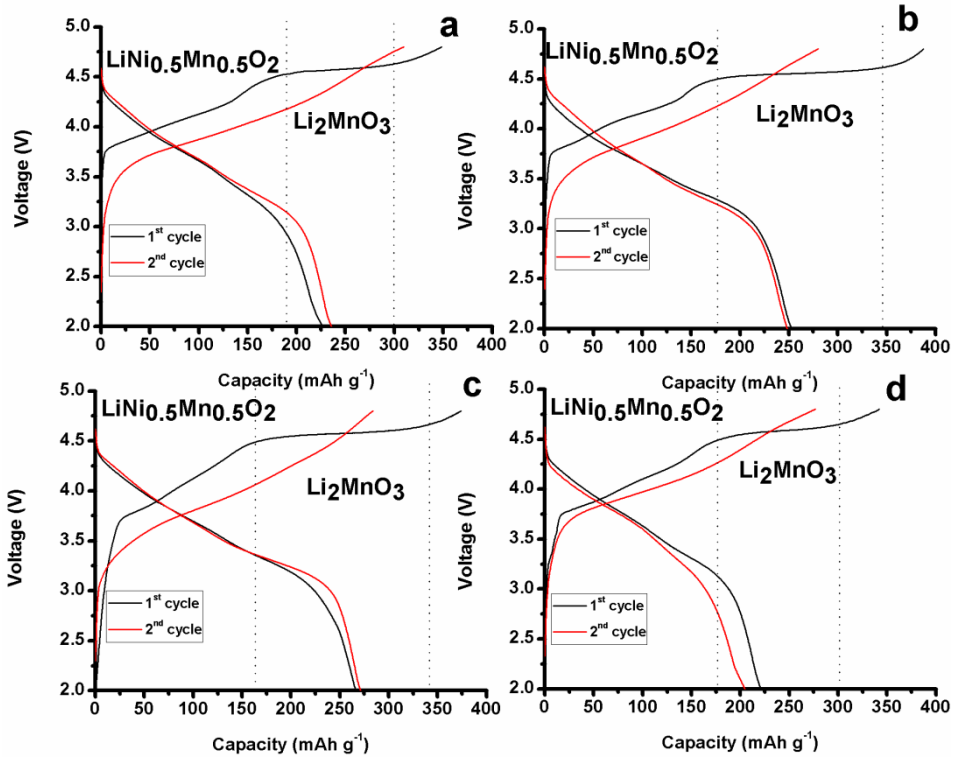

Fig. 5. First-second charge/discharge voltage profiles of $Li_{1.2}Mn_{0.6}Ni_{0.2}O_2$ between 2.0 V – 4.8 V at 20 mA g^{-1}.

To determine the capacity potential of the as synthesized materials as possible energy storage cathode materials in Lithium ion cells, their performances in coin cells were evaluated. Fig. 5 summarizes the initial-second charge/discharge profiles for the as synthesized $Li_{1.2}Mn_{0.6}Ni_{0.2}O_2$ at 20 mA g^{-1} current density between 2.0 V and 4.8 V respectively. All cathode materials showed good stability at starting high potentials of 4.8 V. These materials show high discharge capacities at potentials > 4.5 V at 20 mA g^{-1}. The initial charge and discharge for pH 10.0 is 373 mAh g^{-1} and 266 mAh g^{-1} respectively, making this cathode material 71% coulombic efficient. However coulombic efficiencies for the other materials were 65% on average. Upon the first discharge cycle, all cathode materials suffered capacity loss as expected for Li_2MnO_3 based composites and was similar to the results reported by other group studying these types of composite materials [42]. The large capacity loss during the initial cycle was reported to be associated with the complete loss of Li_2O during

activation of Li_2MnO_3 component [43]. All electrodes exhibit a sloping voltage profile below 4.4 V, followed by a relatively long plateau around 4.5 V during the first charge process. The sloping voltage profile can be attributed to the oxidation of Ni^{2+} to Ni^{4+} ions in the $LiMn_{0.5}Ni_{0.5}O_2$ component and the 4.5 V plateau voltage profile rises from the simultaneous irreversible removal of Li^+ ions and oxygen (Li_2O) [15, 43]. The capacity produced by $LiMn_{0.5}Ni_{0.5}O_2$ component was just above 150 mAh g^{-1} for all four cathode materials a value previously reported for $LiMn_{0.5}Ni_{0.5}O_2$ [44]. The capacity was produced from the sloping voltage profile by Ni^{2+} to Ni^{4+} oxidation in the $LiMn_{0.5}Ni_{0.5}O_2$ component. The long plateau observed relates to the activation of Li_2MnO_3 component converting the material into an electrochemically active material. The process is irreversible as the plateau is absent in the second cycles. The capacity produced by Li_2MnO_3 component as highlighted by the dotted lines was 110 mAh g^{-1}, 125 mAh g^{-1}, 173 mAh g^{-1} and 180 mAh g^{-1} for pH 9.0, pH 10.5, pH 9.5 and pH 10.0 respectively. The capacity due to Li_2MnO_3 is very low compared to its theoretical capacity of 460 mAh g^{-1}, for pH 10.0 only 39% capacity of Li_2MnO_3 component was produced [45]. All the cells produced discharge capacities more than 200 mAh g^{-1} at 20 mA g^{-1} current densities.

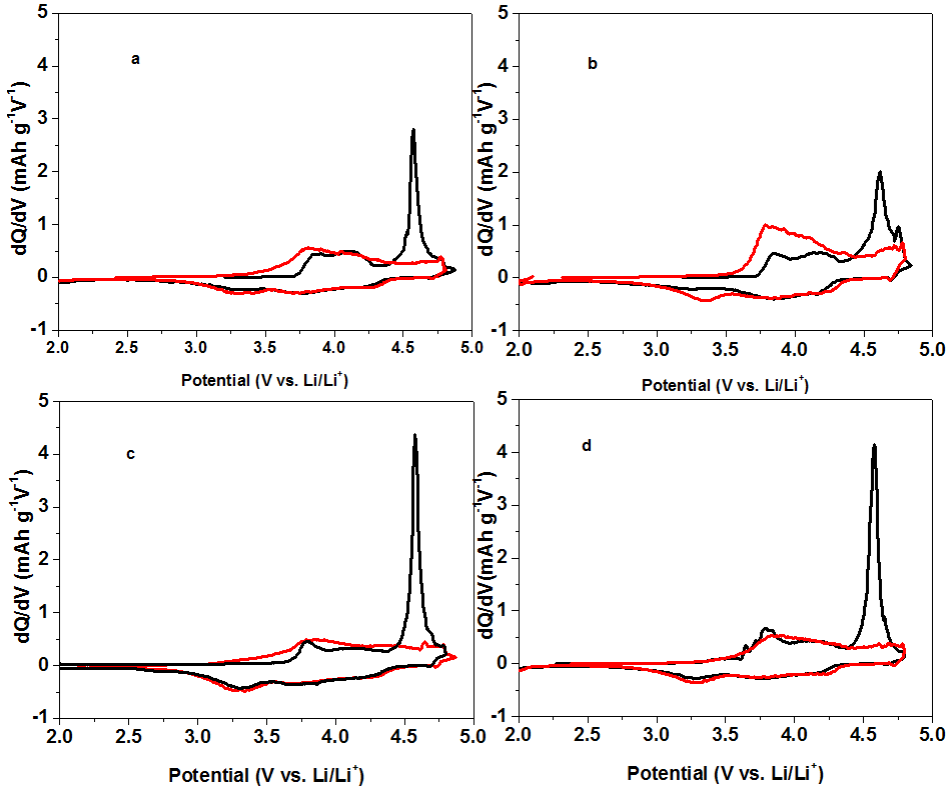

Fig. 6. Differential capacity profiles for the 1st (black) and 2nd (red) charge-discharge cycles of the $Li_{1.2}Mn_{0.6}Ni_{0.2}O_2$ material at (a) pH 9.0, (b) 9.5, (c) 10.0 and (d) 10.5 respectively.

The redox processes that take place during charge/discharge are highlighted by the differential capacity versus voltage plots for the first and second cycle of the prepared cathode materials are shown in Fig. 6. The first cycle consists of two main anodic peaks and corresponding two main cathodic peaks observed for all four cathode materials. During the first charge, the first prominent doublet anodic peak between 3.8 V and 4.2 V is observed for pH 9.0 and pH 9.5, however the doublet becomes slightly resolved into one peak as pH increases to pH 10.0 and pH 10.5. The first peak is reported to be associated with the oxidation of Ni^{2+} to Ni^{4+} which is from the $LiMn_{0.5}Ni_{0.5}O_2$ and simultaneous extraction of lithium which also corresponds to the sloping voltage $\leq$ 4.4 V observed in Fig. 5 profiling first charge/discharge of the cathode materials [46]. The second large peak at around 4.6 V (observed for all four samples) can be attributed to the activation of Li_2MnO_3 component of the composite material by the irreversible removal of Li^+ and O (Li_2O) which corresponds to

the plateaus seen in Fig. 5 for all cathode materials prepared respectively. During the second charge step, only one anodic peak for all cathode materials was observed at 3.8 V, the peak that was observed at around 4.6 V during the first charge completely disappeared, confirming that the lithia (Li_2O) removed in the first cycle is irreversible [47]. During the second charge the anodic peak at 3.8 V for materials pH 9.5 and 10.0 retained its position, while for pH 9.0 and pH 9.5 the peak at 3.8 V shifted to 3.65 V and 3.75 V respectively. The results suggests that the material's structure and/or their electrode/electrolyte interface modifications are negligible for the samples made at pH 10.0 and pH 10.5 since the main anodic peak did not shift significantly. On discharging the cells, the peak at about 3.8 V is due to Ni^{4+} reduction to Ni^{2+} and at 3.2V observed for all four materials is attributed to the Mn^{4+} reduction to Mn^{3+} [48, 49]. It is also important to note that the materials produced in this study are stable towards layered-to-spinel phase transformation, this is confirmed by the absence of the peak at 2.8V which has been reported to symbolize the formation of spinel phase [50]. This observation is consistent throughout all four materials.

The Electrochemical Impedance Spectroscopy (EIS) of the cells with the cathode materials made at different pH can give some insight into the internal electrochemistry processes and reaction kinetics of the lithium ion diffusion through the active materials [51]. The semicircle observed in the high frequency region is due to the formation of solid-electrolyte interface (SEI) and the low-frequency tail, also known as the Warburg factor gives information on the Li^+ ion diffusion process for positive electrode [52]. The impedance of the as-prepared cathode materials measured at two points, before cycling (black) and after 20 cycles (red) between 2.0 V- 4.8 V is expressed as Nyquist plots as shown in Fig. 7. One high frequency semicircle was observed for both before and after cycling and the low-frequency tail is also observed. Before charging the ions from both electrodes accumulates in the interface because there is no enough energy to move ions to either the cathode or anode and release electrons

and this may cause SEI resistance. Before charging the semicircle observed in the high frequency is mainly due to R_{ct} (charge transfer resistance) because of the accumulation of charge between two electrodes [52, 53].

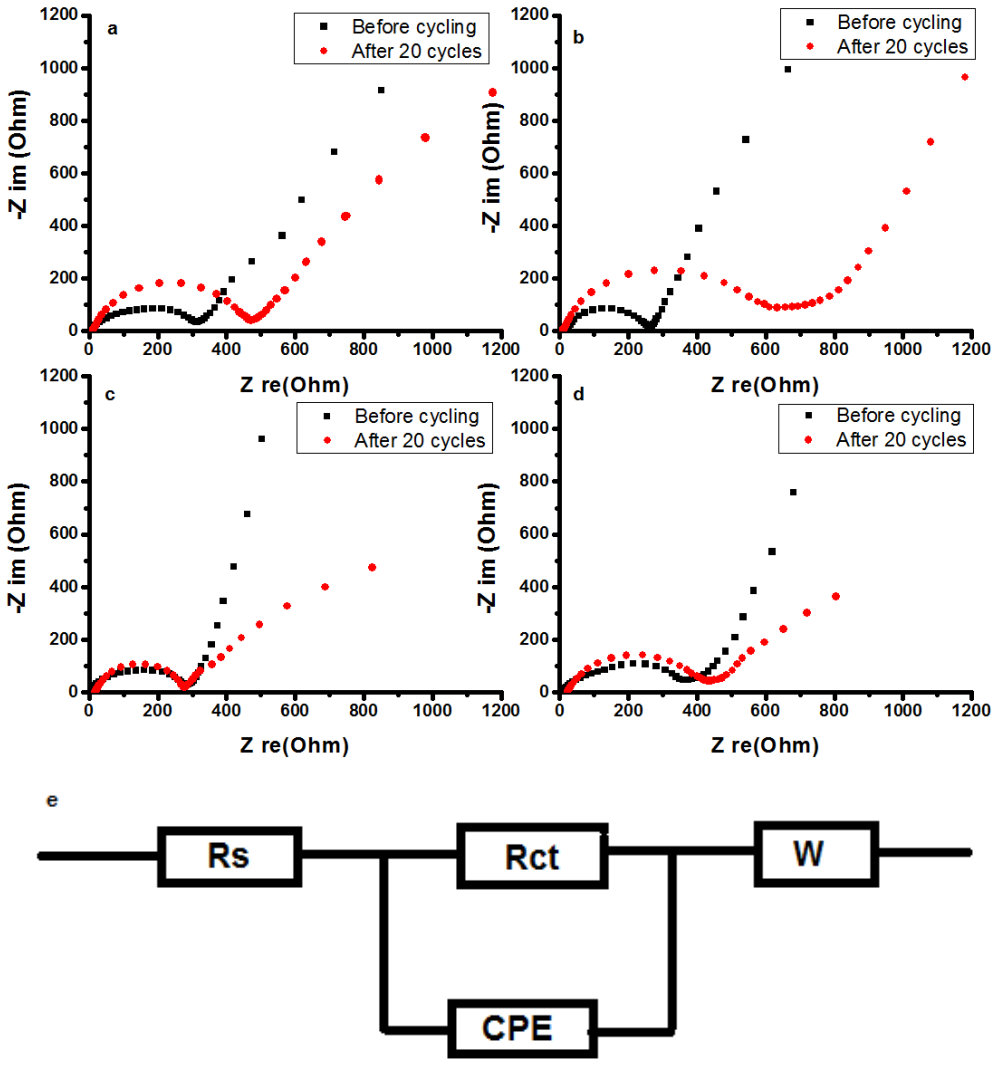

Fig. 7. Nyquist plots of the impedance of the of $Li_{1.2}Mn_{0.6}Ni_{0.2}O_2$ materials at (a) pH 9.0, (b) 9.5 (c) 10.0 and (d) 10.5 before charging and after 20 cycles and (e) the equivalent circuit .

As seen in the table below the R_{ct} and R_s values before cycling are low which is expected because SEI has not yet formed and there is no resistance due to charge transfer happening. Upon cycling both values almost doubled except for pH 10.0 material almost not increasing

at all, R_s (4.715 ± 0.3261) before and (7.003 ± 0.3309) after cycling. The R_{ct} value decreased upon cycling for pH 10.0 (185.6 ± 0.4007) before and (131.1 ± 0.402) meaning that this material is highly conductive and possess faster electrochemical reactions [54]. The electrochemical results in Fig. 5 and 7 are in agreement with this observation as the material delivered higher capacity compared to other materials. The Warburg resistance before charging for pH 10.0 was high due to no Li^+ diffusion at this point and upon cycling the resistance decreased, this therefore suggest that Li^+ diffusion rate is much high with applied voltage. R_{ct} value increased dramatically for pH 10.5 after 20 cycles from 194.8 ± 0.399 to 343.8 ± 0.3995 this explain lowest capacity observed during 1st cycling for the material. However the Warburg function for pH 10.0 deviated much after 20 cycles compared to other materials, this may suggest the deterioration of the material or build-up of capacitance on the surface of the material. In summary from these results it can be concluded that LMR-TM cathode materials possess internal resistance before charge mainly in the form of charge transfer resistance as large R_{ct} values where observed before charging cycling. The R_s values are reasonably low and indicate that the rate of SEI formation for these materials is slow; this therefore suggests that good cycling performance should be expected for these materials.

Table 4: EIS parameters for the $Li_{1.2}Mn_{0.6}Ni_{0.2}O_2$ materials fitted using R_1+C_2 / R_2+W_3 equivalent electrical circuit model.

Sample name	R_s (Ω)	R_{ct} (Ω)	CPE (μF)	Ws (ohm.$s^{-1/2}$)
Before cycling				
pH 9.0	12.15 ± 0.3169	228.3 ± 0.3993	1.6×10^{-6} ± 14.86×10^{-9}	203.8 ± 0.04998
pH 9.5	10.87 ± 0.2894	308 ± 0.4002	1.048×10^{-6} ± 7.244×10^{-9}	130.6 ± 0.04897
pH 10.0	4.715 ± 0.3261	185.6 ± 0.4007	1.632×10^{-6} ± 18.77×10^{-9}	170.5 ± 0.04846
pH 10.5	5.299 ± 0.3181	194.8 ± 0.399	1.963×10^{-6} ± 21.57×10^{-9}	166.4 ± 0.05045
After 20 cycles				
pH 9.0	25.72 ± 0.319	203.6 ± 0.3993	1.974×10^{-6} ± 20.49×10^{-9}	158.7 ± 0.05077
pH 9.5	45.85 ± 0.324	529 ± 0.3988	1.974×10^{-6} ± 7.644×10^{-9}	207.3 ± 0.05997
pH10.0	7.003 ± 0.3309	131.1 ± 0.402	2.001×10^{-6} ± 32.74×10^{-9}	106.5 ± 0.04736
pH 10.5	24.66 ± 0.2866	343.8 ± 0.3995	3.368×10^{-6} ± 20.14×10^{-9}	102.8 ± 0.06119

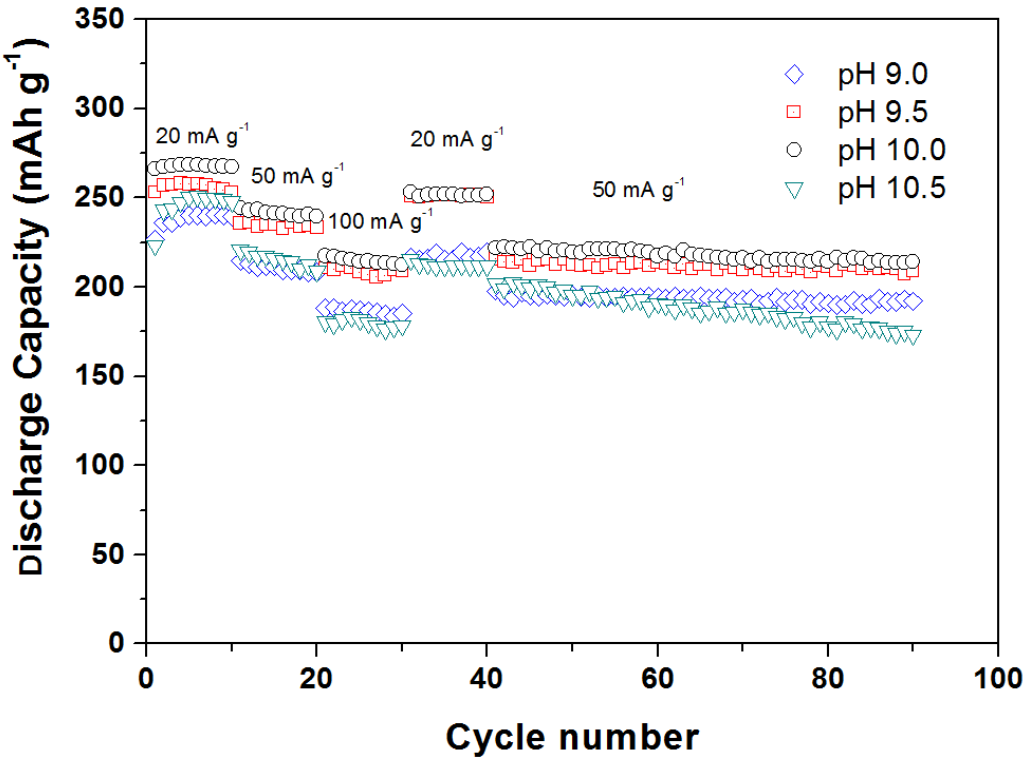

Fig.8. Performances of $Li_{1.2}Mn_{0.6}Ni_{0.2}O_2$ materials discharged at 20 mA g^{-1}, 50 mA g^{-1} and 100 mA g^{-1} in the voltage range 2.0 V to 4.8.

$Li_{1.2}Mn_{0.6}Ni_{0.2}O_2$ cathode materials were cycled at different current densities beginning with 20 mA g^{-1}, 50 mA g^{-1} and 100 mA g^{-1} for 10 cycles per current density followed by another 10 cycles at 20 mA g^{-1} respectively. This was followed by a 50 cycle test at 50 mA g^{-1}, all cycle tests were done between 2.0 V and 4.8 V voltage limits resulting in a total of 90 cycles. The results showed that the cells made with the various cathode materials achieved greater than 200 mAh g^{-1}. The cells also showed good capacity retention properties with about 95% capacity recovery when cycled at the initial current density 20 mA g^{-1} after 30 cycles. From the graph it is evident that capacity decreases steadily with increasing current densities. Materials pH 9.5 and pH 10.0 further delivered > 200 mAh g^{-1} capacity even when charged at

100 mA g^{-1} current density and generally all cathode materials delivered stable capacity even at higher current densities. The cathode material at pH 10.0 delivered the best rate capability performance, with capacities > 220 mAh g^{-1} at all current densities presented in Fig. 7. These results further prove that there is little to non electrode/electrolyte interface modifications, as the cathode materials displayed stable cycling performances.

The cells were cycled further at 50 mA g^{-1} current density between 2.0 V and 4.8 V for 50 more cycles to study the cycling performance/stability of the cathode materials. It is evident that all the cells gave the steady discharge capacity from the 41^{st} cycle to the 90^{th}. All the materials show great capacity retention with no or negligible capacity fade, > 90% capacity retention was observed. Three materials pH 9.5, pH 10.0 and pH 10.5 delivered > 200 mAh g^{-1} discharge capacity steadily over 50 cycles, a great characteristic needed for cathode materials. The material at pH 10.0 demonstrated exceptional cycling performance delivering about 230 mAh g^{-1} over 50 cycles, exhibiting 93% capacity retention. This therefore suggests that these materials do not only deliver high discharge capacities during the 1^{st} and 2^{nd} cycles; even when cycled for longer periods there is great capacity retention. The prepared materials possess intrinsic high capacities with great cycling stability and capacity retention.

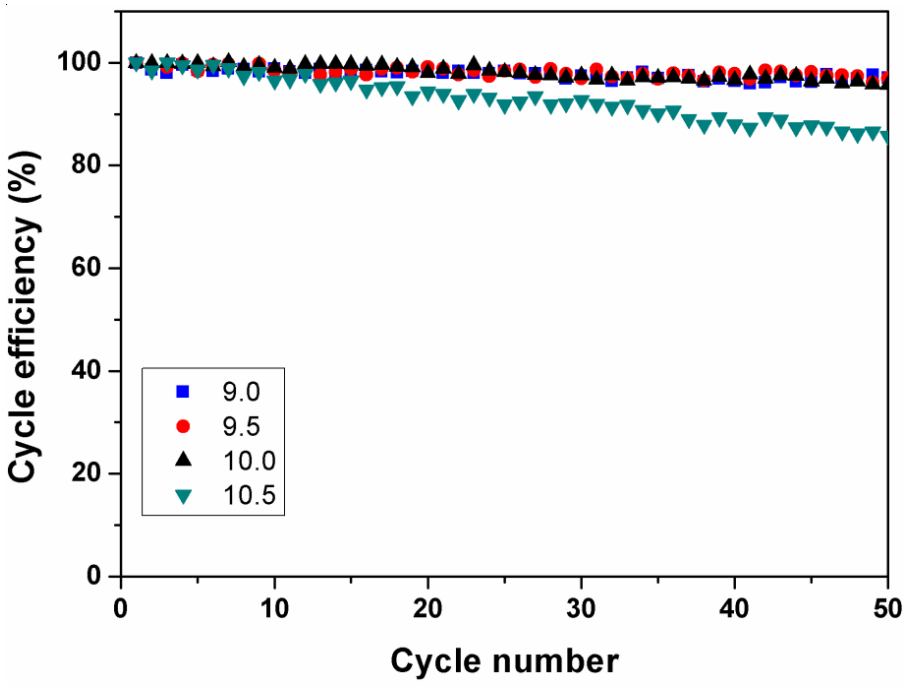

Fig. 9. Cycling efficiency over 50 cycles for $Li_{1.2}Mn_{0.6}Ni_{0.2}O_2$ materials discharged at 50 mA g^{-1}.

Fig. 9 illustrates the cycling efficiency of the $Li_{1.2}Mn_{0.6}Ni_{0.2}O_2$ cathode materials at pH 9.0, pH 9.5, pH 10.0 and pH 10.5 using the cycling performance data of cells discharged at 50 mA g^{-1} as shown in Fig. 8. As alluded above and as seen in the cycling efficiency graph above, all cathode materials have > 90% cycling efficiency after 50 cycles. This therefore suggests that the one pot synthesis co-precipitation method produced stable cathode materials with particle surfaces stable towards harsh electrolyte/electrode reaction. Composite materials of this nature when charged above 4.6 V tend to react with the harsh electrolyte and compromise the durability and subsequently the cycle life of the battery which is not the case with the composite materials reported here. There have been various approaches to combat the harsh electrolyte/electrode reaction, coating/doping the composites materials[2]. The synthesis method used however produced stable particles with no need for coating/doping the particles surfaces. It is also important to highlight that for each cycle the cathode materials

(pH 9.0, pH 9.5 and pH 10.0) retained > 90% capacity with an exception of pH 10.5 showing gradual capacity decreases with cycling.

4. Conclusions

The cathode materials $Li_{1.2}Mn_{0.6}Ni_{0.2}O_2$ were successfully synthesized through a facile modified co-precipitation process at different pH values and annealed at 900 ℃. Structural and morphology analysis of the cathode materials was done using XRD, TEM, BET, ICP-MSand SEM. Material prepared at pH 10.0 had the closest composition to the proposed theoretical composition as confirmed by the ICP-MS and possessed highest surface area. Overall the cathode material at pH 10.0 exhibits the best electrochemical performance at 20 mA g^{-1}, 50 mA g^{-1} and 100 mA g^{-1} current densities and high capacity retention post 90 cycles. All the materials produced displayed a steady cycling at high potentials and displayed good rate performance. The electrochemical performance suggests that the as-developed LMR-TM materials are promising for development towards high capacity lithium ion battery applications and the synthesis method used is suitable to produce homogenous LMR-TM cathode materials.

Acknowledgements

The authors thank the National Research Foundation of South Africa (NRF) and the Council for Scientific and Industrial Research for funding, Nelson Mandela Metropolitan University for academic support.

References

[1] J.J. Chen, Recent Progress in Advanced Materials for Lithium Ion Batteries, Materials, 6 (2013) 156-183.
[2] C. Kim, P.J. Phillips, L. Xu, A. Dong, R. Buonsanti, R.F. Klie, J. Cabana, Stabilization of battery electrode/electrolyte interfaces employing nanocrystals with passivating epitaxial shells, Chemistry of Materials, 27 (2014) 394-399.

[3] F. Schipper, E.M. Erickson, C. Erk, J.-Y. Shin, F.F. Chesneau, D. Aurbach, Review—Recent Advances and Remaining Challenges for Lithium Ion Battery Cathodes: I. Nickel-Rich, LiNixCoyMnzO2, Journal of The Electrochemical Society, 164 (2017) A6220-A6228.
[4] J. Tarascon, W. McKinnon, F. Coowar, T. Bowmer, G. Amatucci, D. Guyomard, Synthesis Conditions and Oxygen Stoichiometry Effects on Li Insertion into the Spinel LiMn2 O 4, Journal of The Electrochemical Society, 141 (1994) 1421-1431.
[5] K.Y. Nam Long Doan, Tuan K.A. Hoang and Pu Chen, Recent development in synthesis of xLi2MnO3.(1-x)LiMO2 (M=Ni, Co, Mn) cathode powders for high energy lithium rechargeable batteries, Frontiers in Energy Research, 2 (2014) 1-23.
[6] W.-b. Luo, L. Wen, H.-z. Luo, R.-s. Song, Y.-c. Zhai, C. Liu, F. Li, Carbon nanotube-modified LiFePO4 for high rate lithium ion batteries, New Carbon Materials, 29 (2014) 287-294.
[7] L. Wen, X. Hu, H. Luo, F. Li, H. Cheng, Open-pore LiFePO4/C microspheres with high volumetric energy density for lithium ion batteries, Particuology, (2015).
[8] X. Liu, T. Huang, A. Yu, Fe doped Li 1.2 Mn 0.6-x/2 Ni 0.2-x/2 Fe x O 2 (x≤ 0.1) as cathode materials for lithium-ion batteries, Electrochimica Acta, 133 (2014) 555-563.
[9] Y. Li, Y. Mao, T. Zhan, C. Li, S. Xiao, Effects of aluminium and sodium co-doping on the structural and electrochemical performances of the spinel LiMn2O4 cathode materials, Micro & Nano Letters, 11 (2016) 430-432.
[10] X. Xiang, J.C. Knight, W. Li, A. Manthiram, Understanding the effect of Co3+ substitution on the electrochemical properties of lithium-rich layered oxide cathodes for lithium-ion batteries, The Journal of Physical Chemistry C, 118 (2014) 21826-21833.
[11] X. Guan, B. Ding, X. Liu, J. Zhu, C. Mi, X. Zhang, Enhancing the electrochemical performance of Li1. 2Ni0. 2Mn0. 6O2 by surface modification with nickel–manganese composite oxide, Journal of Solid State Electrochemistry, 17 (2013) 2087-2093.
[12] M.M. Thackeray, S.-H. Kang, C.S. Johnson, J.T. Vaughey, R. Benedek, S. Hackney, Li 2 MnO 3-stabilized LiMO 2 (M= Mn, Ni, Co) electrodes for lithium-ion batteries, Journal of Materials chemistry, 17 (2007) 3112-3125.
[13] C.S. Johnson, N. Li, C. Lefief, M.M. Thackeray, Anomalous capacity and cycling stability of xLi 2 MnO 3·(1− x) LiMO 2 electrodes (M= Mn, Ni, Co) in lithium batteries at 50 C, Electrochemistry Communications, 9 (2007) 787-795.
[14] J.-S. Kim, C.S. Johnson, J.T. Vaughey, M.M. Thackeray, S.A. Hackney, W. Yoon, C.P. Grey, Electrochemical and Structural Properties of x Li2M'O3⊙(1-x) LiMn0. 5Ni0. 5O2 Electrodes for Lithium Batteries (M'= Ti, Mn, Zr; 0≤ x⊠ 0.3), Chemistry of Materials, 16 (2004) 1996-2006.
[15] M.M. Thackeray, C.S. Johnson, J.T. Vaughey, N. Li, S.A. Hackney, Advances in manganese-oxide 'composite'electrodes for lithium-ion batteries, Journal of Materials Chemistry, 15 (2005) 2257-2267.
[16] S.-H. Kang, M. Thackeray, Stabilization of xLi2MnO3·(1− x) LiMO2 Electrode Surfaces (M= Mn, Ni, Co) with Mildly Acidic, Fluorinated Solutions, Journal of the Electrochemical Society, 155 (2008) A269-A275.
[17] F. Wu, H. Wang, Y. Bai, Y. Li, C. Wu, G. Chen, L. Liu, Q. Ni, X. Wang, J. Zhou, Hierarchical microspheres and nanoscale particles: Effects of morphology on electrochemical performance of Li 1.2 Mn 0.54 Ni 0.13 Co 0.13 O 2 cathode material for lithium-ion batteries, Solid State Ionics, 300 (2017) 149-156.
[18] J.X. Wang, L. Wang, X.M. He, J.J. Li, Z.J. Dai, J.L. Wang, One-step Hydrothermal Synthesis of Li1.24Mn0.66Ni0.1O2 Cathode for Lithium-ion Batteries, Int J Electrochem Sc, 11 (2016) 333-342.
[19] J.X. Wang, R.M. Gu, Y.P. Zhang, B.J. Yu, C.Y. Wang, M.W. Li, Structure and Delithiation/Lithiation of the Lithium-Rich Layered Oxide Li Li0.23Ni0.15Mn0.62 O-2 as Cathode Material, Int J Electrochem Sc, 12 (2017) 8095-8105.
[20] B. Seteni, N. Rapulenyane, J.C. Ngila, S. Mpelane, H. Luo, Coating effect of LiFePO 4 and Al 2 O 3 on Li 1.2 Mn 0.54 Ni 0.13 Co 0.13 O 2 cathode surface for lithium ion batteries, Journal of Power Sources, 353 (2017) 210-220.

[21] S.-H. Kang, M.M. Thackeray, Enhancing the rate capability of high capacity xLi 2 MnO 3·(1− x) LiMO 2 (M= Mn, Ni, Co) electrodes by Li–Ni–PO 4 treatment, Electrochemistry Communications, 11 (2009) 748-751.
[22] M. Kunduraci, G. Amatucci, Synthesis and characterization of nanostructured 4.7 V Li x Mn1. 5Ni0. 5O4 spinels for high-power lithium-ion batteries, Journal of The Electrochemical Society, 153 (2006) A1345-A1352.
[23] S.-H. Park, H.-S. Shin, S.-T. Myung, C. Yoon, K. Amine, Y.-K. Sun, Synthesis of nanostructured Li [Ni1/3Co1/3Mn1/3] O2 via a modified carbonate process, Chemistry of materials, 17 (2005) 6-8.
[24] Q. Sun, Z.-X. Wang, X.-H. Li, H.-J. Guo, W.-J. Peng, Comparison of LiNi0. 5Mn1. 5O4 cathode materials prepared by different coprecipitation methods, Transactions of Nonferrous Metals Society of China, 17 (2007) s917-s922.
[25] D. Wang, Y. Huang, Z. Huo, L. Chen, Synthesize and electrochemical characterization of Mg-doped Li-rich layered Li [Li 0.2 Ni 0.2 Mn 0.6] O 2 cathode material, Electrochimica Acta, 107 (2013) 461-466.
[26] Y. Zhao, C. Zhao, H. Feng, Z. Sun, D. Xia, Enhanced electrochemical performance of Li [Li0. 2Ni0. 2Mn0. 6] O2 modified by manganese oxide coating for lithium-ion batteries, Electrochemical and Solid-State Letters, 14 (2011) A1-A5.
[27] Y. Wang, Z. Yang, Y. Qian, L. Gu, H. Zhou, New Insights into Improving Rate Performance of Lithium-Rich Cathode Material, Advanced Materials, 27 (2015) 3915-3920.
[28] H. Kobayashi, H. Sakaebe, H. Kageyama, K. Tatsumi, Y. Arachi, T. Kamiyama, Changes in the structure and physical properties of the solid solution LiNi 1− x Mn x O 2 with variation in its composition, Journal of Materials chemistry, 13 (2003) 590-595.
[29] P. Strobel, B. Lambert-Andron, Crystallographic and magnetic structure of Li2MnO3, Journal of Solid State Chemistry, 75 (1988) 90-98.
[30] S.K. Jung, H. Gwon, J. Hong, K.Y. Park, D.H. Seo, H. Kim, J. Hyun, W. Yang, K. Kang, Understanding the degradation mechanisms of LiNi0. 5Co0. 2Mn0. 3O2 cathode material in lithium ion batteries, Advanced Energy Materials, 4 (2014).
[31] Y. Hinuma, Y.S. Meng, K. Kang, G. Ceder, Phase transitions in the LiNi0. 5Mn0. 5O2 system with temperature, Chemistry of Materials, 19 (2007) 1790-1800.
[32] K.A. Jarvis, Z. Deng, L.F. Allard, A. Manthiram, P.J. Ferreira, Atomic structure of a lithium-rich layered oxide material for lithium-ion batteries: evidence of a solid solution, Chemistry of materials, 23 (2011) 3614-3621.
[33] F. Wu, X. Zhang, T. Zhao, L. Li, M. Xie, R. Chen, Multifunctional AlPO4 Coating for Improving Electrochemical Properties of Low-Cost Li [Li0. 2Fe0. 1Ni0. 15Mn0. 55] O2 Cathode Materials for Lithium-Ion Batteries, ACS applied materials & interfaces, 7 (2015) 3773-3781.
[34] K.R. Prakasha, M. Sathish, P. Bera, A.S. Prakash, Mitigating the Surface Degradation and Voltage Decay of Li1. 2Ni0. 13Mn0. 54Co0. 13O2 Cathode Material through Surface Modification Using Li2ZrO3, ACS Omega, 2 (2017) 2308-2316.
[35] J. Wilcox, S. Patoux, M. Doeff, Structure and Electrochemistry of LiNi1⁄ 3Co1⁄ 3− y M y Mn1⁄ 3O2 (M= Ti, Al, Fe) Positive Electrode Materials, Journal of The Electrochemical Society, 156 (2009) A192-A198.
[36] Y. Wu, A. Manthiram, Structural stability of chemically delithiated layered (1− z) Li [Li 1/3 Mn 2/3] O 2–zLi [Mn 0.5− y Ni 0.5− y Co 2y] O 2 solid solution cathodes, Journal of Power Sources, 183 (2008) 749-754.
[37] Y. Meng, G. Ceder, C. Grey, W.-S. Yoon, Y. Shao-Horn, Understanding the Crystal Structure of Layered LiNi0. 5Mn0. 5 O 2 by Electron Diffraction and Powder Diffraction Simulation, Electrochemical and Solid-State Letters, 7 (2004) A155-A158.
[38] Y. Meng, G. Ceder, C. Grey, W.-S. Yoon, M. Jiang, J. Breger, Y. Shao-Horn, Cation Ordering in Layered O3 Li [Ni x Li1/3-2 x/3Mn2/3-x/3] O2 (0≤ x≤ 1/2) Compounds, Chemistry of Materials, 17 (2005) 2386-2394.

[39] H. Deng, I. Belharouak, Y.-K. Sun, K. Amine, Li x Ni 0.25 Mn 0.75 O y (0.5≤ x≤ 2, 2≤ y≤ 2.75) compounds for high-energy lithium-ion batteries, Journal of Materials Chemistry, 19 (2009) 4510-4516.
[40] G.M. Koenig, I. Belharouak, H.M. Wu, K. Amine, Hollow lithiated metal oxide particles as lithium-ion battery cathode materials, Electrochimica Acta, 56 (2011) 1426-1431.
[41] Y. Arachi, H. Kobayashi, S. Emura, Y. Nakata, M. Tanaka, T. Asai, H. Sakaebe, K. Tatsumi, H. Kageyama, Li de-intercalation mechanism in LiNi0. 5Mn0. 5O2 cathode material for Li-ion batteries, Solid State Ionics, 176 (2005) 895-903.
[42] N. Yabuuchi, K. Yoshii, S.-T. Myung, I. Nakai, S. Komaba, Detailed studies of a high-capacity electrode material for rechargeable batteries, Li2MnO3− LiCo1/3Ni1/3Mn1/3O2, Journal of the American Chemical Society, 133 (2011) 4404-4419.
[43] J.-K. Noh, S. Kim, H. Kim, W. Choi, W. Chang, D. Byun, B.-W. Cho, K.Y. Chung, Mechanochemical Synthesis of Li2MnO3 Shell/LiMO2 (M= Ni, Co, Mn) Core-Structured Nanocomposites for Lithium-Ion Batteries, Scientific reports, 4 (2014).
[44] G. Yang, E. Zhao, M. Chen, Y. Cheng, L. Xue, Z. Hu, X. Xiao, F. Li, Mg doping improving the cycle stability of LiNi0. 5Mn0. 5O2 at high voltage, Journal of Solid State Electrochemistry, (2017) 1-9.
[45] M. Nookala, T.R. Penki, S. Duraisamy, Porous Li2MnO3 as a High Capacity and High Rate Capability Cathode Material, Meeting Abstracts, The Electrochemical Society, 2012, pp. 3347-3347.
[46] C.S. Johnson, N. Li, C. Lefief, J.T. Vaughey, M.M. Thackeray, Synthesis, Characterization and Electrochemistry of Lithium Battery Electrodes: x Li2MnO3·(1− x) LiMn0. 333Ni0. 333Co0. 333O2 (0≤ x≤ 0.7), Chemistry of Materials, 20 (2008) 6095-6106.
[47] S.-H. Kang, P. Kempgens, S. Greenbaum, A. Kropf, K. Amine, M. Thackeray, Interpreting the structural and electrochemical complexity of 0.5 Li 2 MnO 3· 0.5 LiMO 2 electrodes for lithium batteries (M= Mn 0.5− x Ni 0.5− x Co 2x, 0≤ x≤ 0.5), Journal of Materials Chemistry, 17 (2007) 2069-2077.
[48] W. Zheng, X. Xu, L. Cheng, M. Shui, J. Shu, S. Gao, Z. Lu, L. Feng, Y. Ren, The intercalation/deintercalation kinetic studies on the structure-integrated cathode material 0.5 Li 2 MnO 3 0.5 LiNi 0.5 Mn 0.5 O 2, Ionics, 19 (2013) 1509-1514.
[49] E.M. Erickson, F. Schipper, T.R. Penki, J.-Y. Shin, C. Erk, F.-F. Chesneau, B. Markovsky, D. Aurbach, recent advances and remaining challenges for lithium ion battery cathodes II. Lithium-rich, xLi2MnO3·(1-x) LiNiaCobMncO2, Journal of The Electrochemical Society, 164 (2017) A6341-A6348.
[50] K.J. Carroll, D. Qian, C. Fell, S. Calvin, G.M. Veith, M. Chi, L. Baggetto, Y.S. Meng, Probing the electrode/electrolyte interface in the lithium excess layered oxide Li 1.2 Ni 0.2 Mn 0.6 O 2, Physical Chemistry Chemical Physics, 15 (2013) 11128-11138.
[51] D. Andre, M. Meiler, K. Steiner, C. Wimmer, T. Soczka-Guth, D. Sauer, Characterization of high-power lithium-ion batteries by electrochemical impedance spectroscopy. I. Experimental investigation, Journal of Power Sources, 196 (2011) 5334-5341.
[52] J. Song, H. Lee, Y. Wang, C. Wan, Two-and three-electrode impedance spectroscopy of lithium-ion batteries, Journal of Power Sources, 111 (2002) 255-267.
[53] L. Wen, J. Liang, C.-M. Liu, J. Chen, Q.-g. Huang, H.-z. Luo, F. Li, Li4Ti5O12 on Graphene for High Rate Lithium Ion Batteries, J Electrochem Soc, 163 (2016) A2951-A2955.
[54] X. He, J. Wang, L. Wang, J. Li, Nano-Crystalline Li1. 2Mn0. 6Ni0. 2O2 Prepared via Amorphous Complex Precursor and Its Electrochemical Performances as Cathode Material for Lithium-Ion Batteries, Materials, 9 (2016) 661.